

# CHEMISTRY

## A European Journal



### Accepted Article

**Title:** Monodisperse Six-Armed Starbursts based on Truxene-Cored Multibranching Oligofluorenes: Design, Synthesis, and Stabilized Lasing Characteristics

**Authors:** Hao Zhang, Xu Liu, Ting-Ting Lu, Peng Lv, and Wen-Yong Lai

This manuscript has been accepted after peer review and appears as an Accepted Article online prior to editing, proofing, and formal publication of the final Version of Record (VoR). This work is currently citable by using the Digital Object Identifier (DOI) given below. The VoR will be published online in Early View as soon as possible and may be different to this Accepted Article as a result of editing. Readers should obtain the VoR from the journal website shown below when it is published to ensure accuracy of information. The authors are responsible for the content of this Accepted Article.

**To be cited as:** *Chem. Eur. J.* 10.1002/chem.201805813

**Link to VoR:** <http://dx.doi.org/10.1002/chem.201805813>

Supported by  
**ACES**

WILEY-VCH

DOI: 10.1002/ ((please add manuscript number))

Article type: (Full Paper)

## Monodisperse Six-Armed Starbursts based on Truxene-Cored Multibranched Oligofluorenes: Design, Synthesis, and Stabilized Lasing Characteristics

Hao Zhang,<sup>†</sup> Xu Liu,<sup>†</sup> Ting-Ting Lu, Peng Lv, and Wen-Yong Lai\*

---

H. Zhang, Dr. X. Liu, T.-T. Lu, P. Lv, and Prof. W.-Y. Lai

Key Laboratory for Organic Electronics and Information Displays (KLOEID) & Institute of Advanced Materials (IAM), Jiangsu National Synergetic Innovation Center for Advanced Materials (SICAM), Nanjing University of Posts & Telecommunications (NUPT), 9 Wenyuan Road, Nanjing 210023, China

E-mail: [iamwylai@njupt.edu.cn](mailto:iamwylai@njupt.edu.cn)

<sup>†</sup>These authors contributed equally to this work.

---

## WILEY-VCH

**ABSTRACT:** A series of monodisperse six-armed conjugated starbursts (**Tr1F**, **Tr2F** and **Tr3F**) containing a truxene core and multibranching oligofluorene bridges capped with diphenylamine (DPA) units has been designed, synthesized, and investigated as robust gain media for organic semiconductor lasers (OSLs). The influence of electron-rich DPA end-groups on their optoelectronic characteristics has been discussed at length. DPA cappers effectively raise HOMO levels of the starbursts, thus enhancing the hole injection and transport ability. Solution-processed electroluminescence devices based on the resulting six-armed starbursts exhibited efficient deep-blue electroluminescence with clear reduced turn-on voltages (3.2~3.5 V). Moreover, the resulting six-armed molecules showed stabilized electroluminescence and amplified spontaneous emission with low thresholds (27.4~63.9 nJ pulse<sup>-1</sup>), high net gain coefficients (80.1~101.3 cm<sup>-1</sup>), and small optical loss (2.6~4.4 cm<sup>-1</sup>). Distributed feedback OSLs made from **Tr3F** exhibited low lasing threshold of 0.31 kW/cm<sup>2</sup> (at 465 nm). The results suggest that the construction of truxene-centered six-armed conjugated starbursts with the incorporation of DPA units can effectively enhance EL properties by precisely regulating the HOMO energy levels, and further optimizing their optical gain properties.

**Keywords:** Organic semiconductor lasers (OSLs); Organic gain media; Conjugated starburst molecules; HOMO levels; Organic light-emitting diodes (OLEDs)

## 1. Introduction

Organic light-emitting devices based on organic  $\pi$ -conjugated semiconductors are receiving increasing attention due to their great promising application in the fundamental field of biological probes, chemical sensors and especially organic light-emitting diodes (OLED)<sup>[1-4]</sup> and organic semiconductor lasers (OSLs).<sup>[5-8]</sup> Over the past decade, great progress made in novel molecular designs of  $\pi$ -conjugated semiconductors, such as thermally activated delayed fluorescence (TADF) materials,<sup>[2]</sup> aggregation-induced emission (AIE) materials,<sup>[3]</sup> and room-temperature phosphorescence (RTP) materials,<sup>[4]</sup> have made an important contribution to the advancement of organic electronics. Among them, OSLs are particularly challenging.<sup>[9]</sup> Especially, electrically pumped OSLs, which ask organic gain materials with good emission efficiency, strong optical gain, low lasing thresholds, and high mobilities, have not been realized yet.<sup>[10-12]</sup> Although many organic emitters show great promise in OLEDs, only a few organic materials can afford low thresholds and high optical gain, which are essential for OSLs. Consequently, it is highly required to develop prominent gain media with superior optical gain and lasing characteristics for OSLs.

As far as we are concerned, the most widely employed materials for OSLs mainly include  $\pi$ -conjugated materials.<sup>[13-15]</sup> Organic materials containing fluorene units have served as attractive candidates as organic optical gain materials due to the high photoluminescence quantum yields (PLQYs), good film-forming abilities, and facile tunability of optical and electrical characteristics by substitution or copolymerization.<sup>[8]</sup> However, these materials tend to form aggregates/excimers, which are detrimental to luminescence efficiency, spectral stability and corresponding electrical characteristics.<sup>[16-18]</sup> To tackle the problems mentioned above, various strategies on incorporating bulky moieties with steric hindrance, constructing starburst architectures, or carefully adjusting the polymer side chain structures have been proposed.<sup>[19-24]</sup> Despite great development in this aspect, it still has a long way to go for achieving electrically pumped OSLs. The design and synthesis of prominent molecules possessing superior thermal stability and optoelectronic characteristics for

OSLs is worthy of attention and effort. Investigation on the relationships between the structures and optoelectronic characteristics is of great importance to provide a deep insight on developing reasonable design strategies for organic gain media with high performance.

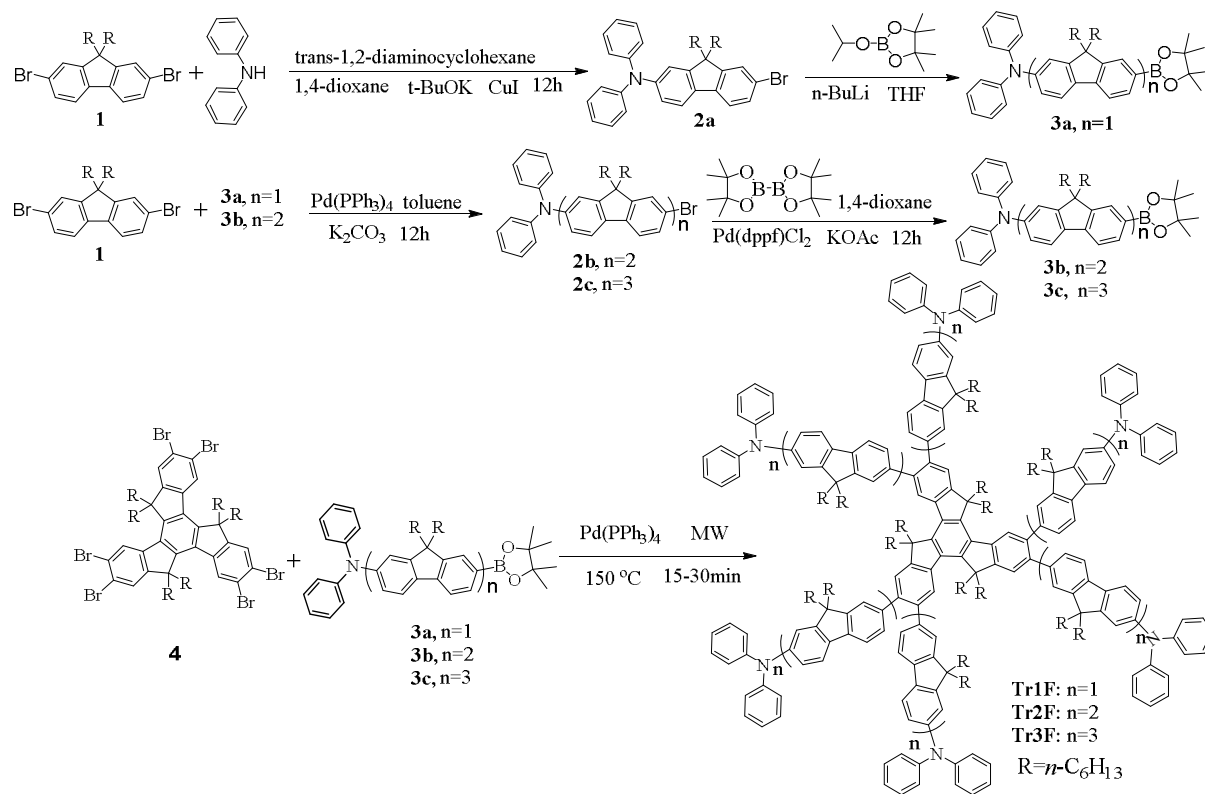
According to our previous studies, a variety of monodisperse  $\pi$ -conjugated starbursts with multifarious cores such as triazatruxene,<sup>[25-29]</sup> truxene,<sup>[30-32]</sup> and pyrene,<sup>[33-37]</sup> have been explored. Such starburst compounds, which combine both the merits of small molecules and polymers, appear rather promising as active materials for OLEDs and OSLs owing to their high chemical purity, excellent stability, facile processibility *via* solution-based methods, good film-forming ability, promising lasing properties. Among them, truxene-centered multiarmed starburst derivatives are rather attractive as robust organic emitters.<sup>[38,39]</sup> A set of monodisperse six-armed starburst molecules composed of truxene core and oligofluorene arms (**Tr1–Tr4**)<sup>[38]</sup> exhibited not only stable pure-deep-blue emission, but also excellent lasing characteristics with ultralow lasing threshold ( $E_{\text{th}}^{\text{laser}} \approx 0.4 \text{ nJ/pulse}$ ,  $1.3 \mu\text{J cm}^{-2}$ ) due to depressed aggregation tendency. Nevertheless, their electrical behaviors remain to be further improved to meet the challenges for electrically pumped OSLs, which require high charge carrier mobility for high current injection and transport. Especially, the energy level mismatch between HOMO levels of **Tr1–Tr4** (-5.66 ~ -5.74 eV) and the work function of the common anodes (i.e. ITO: 4.5~4.8 eV) generally causes weak carrier injection and transport, which restricts their practical applications in OLEDs and electrically pumped OSLs.

In this contribution, on continuing our further efforts, a novel series of monodisperse six-armed starburst conjugated molecules (**Tr1F**, **Tr2F** and **Tr3F**) based on truxene core with six oligofluorenes as bridge arms end-capped with diphenylamine (DPA) units have been designed, synthesized, and investigated, aiming at developing optimal gain materials possessing promising electrical characteristics to overcome obstacles of OSLs. DPA units as the electron-donating arylamine moieties were incorporated into the six-armed starburst molecular structures because of

their strong electron-donating characteristics, which are beneficial for raising the HOMO levels and precisely modulating main electrical behaviors of the resulting molecules.<sup>[40-46]</sup> For instance, Neher et al. achieved blue OLEDs with high efficiency and excellent color stability by end-capping of polyfluorene homopolymer with DPA.<sup>[47]</sup> Oligofluorenes were incorporated with the aim to increase PLQYs and film-forming characteristics.<sup>[48,49]</sup> The effect of the structural modification and the incorporation of DPA moieties on their physical and optoelectronic characteristics, especially lasing characteristics have been systematically explored. Solution-processed OLEDs based on these starbursts showed relatively low turn-on voltages (3.2~3.5 V) and bright emission (1974~3478 cd m<sup>-2</sup>). Ultra-low amplified spontaneous emission (ASE) thresholds (27.4~63.9 nJ pulse<sup>-1</sup>), high net gain coefficients (80.1~101.3 cm<sup>-1</sup>), outstanding ASE stability upon temperature, and low loss properties (2.6~4.4 cm<sup>-1</sup>) were achieved. It is indicated that the design strategy with incorporating DPA end-groups is advantageous for enhancing the efficiency by precisely adjusting the HOMO levels as well as optimizing the gain characteristics of the resulting molecules. Combining the large gain and small waveguide loss with outstanding stability, the resulting six-armed starburst conjugated molecules manifest great potentials as robust gain media for OSLs.

## 2. Experimental

The synthetic routes of DPA-capped six-armed truxene derivatives, **Tr1F**, **Tr2F**, and **Tr3F**, are depicted in Scheme 1. The synthesis of the target starbursts adopted a stepwise convergent synthetic strategy, including microwave-assisted Pd-catalytic multiple Suzuki coupling reaction of DPA-functionalized oligofluorene arms with the 2,3,7,8,12,13-hexaaryltruxene core structure. The Suzuki cross-coupling reaction assisted by microwave irradiation ((30 min at 150 °C) gave the resulting materials in 40%–55% yields. The chemical purity and structures of **Tr1F**, **Tr2F**, and **Tr3F** were confirmed by MALDI-TOF mass spectrometry, <sup>1</sup>H NMR and <sup>13</sup>C NMR data (see Figure S19–S27 in the Supporting Information). Details on synthetic processes and measurements can be found in Supporting Information.



Scheme 1. Synthetic routes of Tr1F, Tr2F, and Tr3F.

### 3. Results and discussion

#### 3.1 Thermal and morphological properties

Differential scanning calorimetry (DSC) and thermogravimetric analysis (TGA) experiments were performed to investigate the thermal stabilities of Tr1F, Tr2F, and Tr3F. High  $T_d$  (5% weight loss temperatures) over 410°C for the resulting starbursts (Figure 1) indicated excellent thermal stability, which guaranteed their good thermal stabilities for practical applications. Furthermore, DSC curves suggested glassy morphologies of Tr1F, Tr2F, and Tr3F. With an increment of the oligofluorene length, a slight increase in glass-transition temperature ( $T_g$ ) (85°C for Tr1F, 90°C for Tr2F, 93°C for Tr3F) (inset of Figure 1) was observed. The  $T_g$  results are higher in comparison to those of their corresponding analogues Tr1–Tr3 with no DPA end-groups ( $T_g = 49\text{--}85^\circ\text{C}$ ).<sup>[38,39]</sup> According to wide-angle X-ray diffraction (WAXD) curves (Figure S28), broad amorphous halos with low intensity at around  $2\theta = 22^\circ$  further confirmed the amorphous glassy morphology of the resulting starbursts. According to these results, DPA moieties are advantageous in limiting the

crystallization process and producing amorphous films, thus increasing the thermal stability and morphological stability of the films.

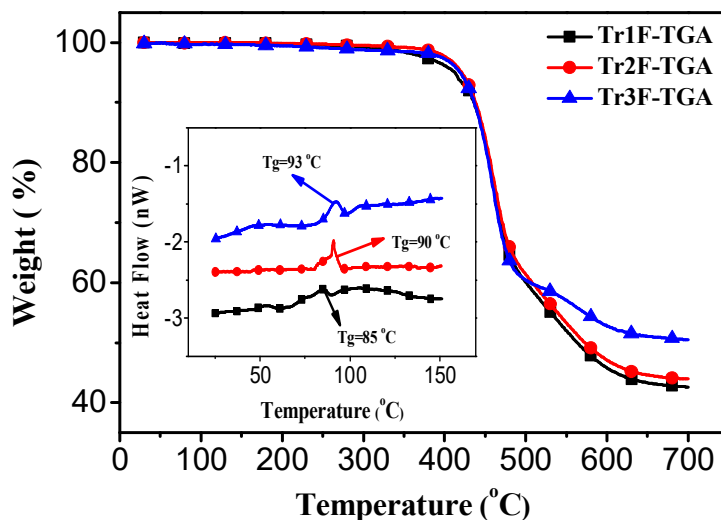


**Figure 1.** TGA thermograms of **Tr1F**, **Tr2F**, to **Tr3F**. Inset: DSC traces.

Atomic force microscopy (AFM) of **Tr1F**, **Tr2F** and **Tr3F** was conducted to investigate the film-forming ability (Figure 2a-c) on quartz substrates. With the increase of the oligofluorene arm length, the film-forming ability was effectively improved, which was confirmed by the surface morphology of pristine **Tr1F**, **Tr2F** and **Tr3F** films. A bit rough film was observed for **Tr1F** film with a root mean-square (RMS) roughness of 1.281 nm, while **Tr2F** and **Tr3F** gave smooth films with RMS roughness of 0.251 and 0.228 nm, respectively.

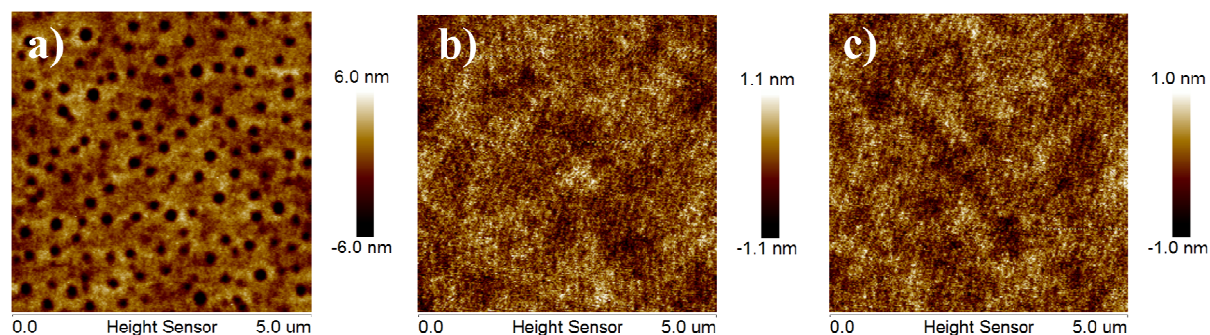


**Figure 2.** AFM images of a) **Tr1F**, b) **Tr2F** and c) **Tr3F**. Scan size is  $2\ \mu\text{m} \times 2\ \mu\text{m}$  and scan rate is 1 Hz at room temperature in  $\text{N}_2$  atmosphere.

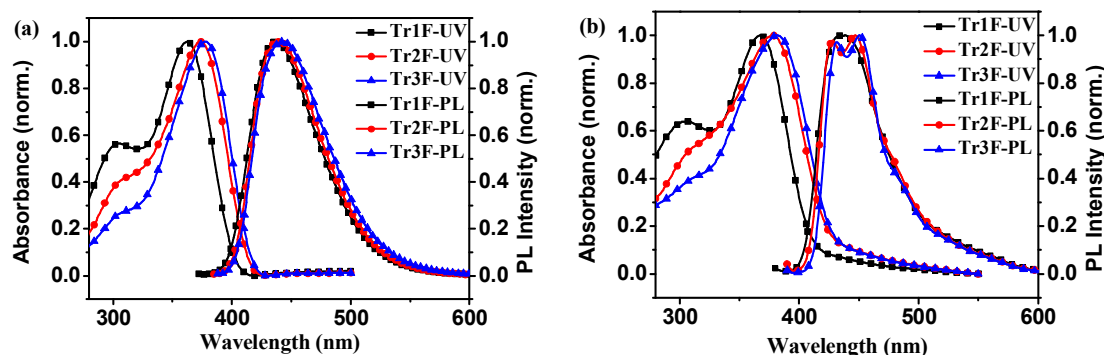


**Figure 3.** Absorption and PL spectra of **Tr1F**, **Tr2F**, **Tr3F** in (a) THF and (b) film.

**Table 1.** Photophysical and electrochemical data of **Tr1F–Tr3F**.

Compd	$\lambda_{\text{abs}}$ (nm)		$\lambda_{\text{em}}$ (nm)		$\tau$ (ns) <sup>c)</sup>		$\Phi_{\text{PL}}$ <sup>d)</sup>		HOMO <sup>e)</sup> /LUMO <sup>e)</sup> (eV)
	THF <sup>a)</sup>	Film <sup>b)</sup>	THF	Film	THF	Film	THF	Film	Film
<b>Tr1F</b>	300,362	304,367	435	438	1.50	0.58(90%) 3.23(10%)	0.63	0.56	-5.17/-2.03
<b>Tr2F</b>	303,373	309,378	438	427,445	1.13	0.38(85%) 2.76(15%)	0.85	0.82	-5.20/-2.08
<b>Tr3F</b>	304,377	311,381	442	430,450	1.03	0.45(88%) 2.63(12%)	0.93	0.89	-5.22/-2.14

<sup>a)</sup> Measured in THF with a concentration of  $10^{-6}$  M; <sup>b)</sup> Measured in solid states; <sup>c)</sup> PL maxima as the excitation wavelength; <sup>d)</sup> Fluorescence quantum yields in films. <sup>e)</sup> Based on the onset of oxidation and reduction potentials.

### 3.2 Photophysical characteristics

The absorption and photoluminescence (PL) spectra of **Tr1F**, **Tr2F**, and **Tr3F** in both tetrahydrofuran (THF) solution ( $10^{-6}$  M) and solid films were recorded (Figure 3, Table 1). These starbursts exhibited bathochromic absorption and PL spectra relative to their analogues **Tr1–Tr3** without DPA end-groups.<sup>[38]</sup> In films, the absorption spectra of **Tr1F–Tr3F** (Figure 3b) remain similar to those in dilute solutions (Figure 3a). The normalized UV–Vis absorption showed two distinctive peaks at 300 and 362 nm for **Tr1F**, 303 and 373 nm for **Tr2F**, and 304 and 377 nm for **Tr3F**, respectively. The peaks of absorption spectra located in the range of 362~377 nm mostly result from  $\pi$ - $\pi^*$  transitions of DPA end-capped arms. Under this circumstance, the absorption peaks

## WILEY-VCH

are gradually red-shifted by extending the length of oligofluorene arm. Additionally, the maxima absorption spectra of each molecule in films exhibit a slight red-shift (4~5 nm) as compared with those in dilute solutions. According to the similar absorption behaviors, the starbursts demonstrate similar ground-state electronic structures, with the absence of large aggregates or conformational changes in the solid-state films. The bulky six-armed starburst architectures with strong steric hindrance are believed to play important roles on effectively inhibiting the intermolecular close packing. The results follow similar trends to the previous studies on truxene derivatives<sup>[38,39]</sup> and DPA dendrimers.<sup>[47]</sup>

PL spectral shapes of **Tr1F–Tr3F** in thin films (Figure. 3b) are different from those in dilute solutions (Figure. 3a). The solution PL emission bands of these starburst molecules show major peaks in the range of 435~442 nm. **Tr1F** showed one main emission peak with a very slightly red-shifted PL band peaked at 438 nm in films, which suggested no obvious intermolecular interactions and intramolecular ordering in films in this system. For **Tr2F** and **Tr3F** in solid films, the major emission peaks located at  $\lambda_{em} = 445$  and 450 nm, respectively, with a shoulder emission at 427 nm. The six-armed bulky architectures likely aid to maintain an isolated-molecule emission induced by increasing the oligofluorene arm length.<sup>[50,51]</sup> This is significant for high luminescence efficiency because intermolecular interactions induced by  $\pi$ - $\pi$  stacking in most conjugated molecules generally depress the luminescence in condensed states. On the basis of the results, the luminescence properties of the resulting starbursts just slightly rely on the arm length. Nevertheless, it appears as a perfect fluorene-based platform for further exploring the influence of structures on the film morphology and resulting optoelectronic characteristics.

Upon excitation at their absorption maxima, **Tr1F**, **Tr2F**, and **Tr3F** manifested high PLQYs of 56%, 82%, and 89% even in films, quite close to those in solutions of 63%, 85%, and 93%, respectively. The results indicate that the bulky six-armed starburst architecture effectively suppresses the intermolecular interactions in solid states. PLQYs for **Tr2F** and **Tr3F** became quite

close, indicating that the effect of the oligofluorene chain on depressing the intramolecular interactions will be passivated with increasing the arm length. This tendency was further confirmed by transient PL characterization in films. According to the PL decay transients of dilute solutions and solid states (Figure S29), the PL decay transients in dilute solutions showed single exponential decays (estimated fluorescence lifetimes ( $\tau$ ) of 1.50 ns, 1.13 ns and 1.03 ns for **Tr1F**, **Tr2F**, and **Tr3F**, respectively), while the PL decay transients in thin films manifested bi-exponential decay profiles, demonstrating  $\tau_1 = 0.58$  ns (90.15%),  $\tau_2 = 3.23$  ns (9.85%) for **Tr1F**,  $\tau_1 = 0.38$  ns (85.15%),  $\tau_2 = 2.76$  ns (14.85%) for **Tr2F**, and  $\tau_1 = 0.45$  ns (88.03%),  $\tau_2 = 2.63$  ns (11.97%) for **Tr3F**, respectively (Table 1).

### 3.3 Electrochemical characteristics

Cyclic voltammetry (CV) was conducted with the aim to study the electrochemical behaviors of **Tr1F**, **Tr2F**, and **Tr3F**. The results are depicted in Figure 4 and listed in Table 1 and Table S1. The onset oxidation potentials ( $E_{ox}$ ) of **Tr1F**, **Tr2F**, **Tr3F** are 0.45, 0.48, and 0.50 eV, respectively. HOMO energy levels of **Tr1F**, **Tr2F**, and **Tr3F** are thus determined as -5.17, -5.20, and -5.22 eV, respectively, which are 0.49~0.52 eV higher than those of their analogues without DPA end-cappers (**Tr1**: -5.66 eV, **Tr2**: -5.70 eV, **Tr3**: -5.74 eV),<sup>[38]</sup> respectively. At the same time, the onset reduction potentials of **Tr1F**, **Tr2F**, and **Tr3F** were measured as -2.69, -2.64, and -2.58 eV, respectively. The corresponding LUMO levels of **Tr1F**, **Tr2F**, and **Tr3F** are calculated to be -2.05, -2.07, and -2.14 eV based on  $E_{LUMO} = - [E_{red} + 4.72]$  eV. The band gaps ( $E_g$ ) of **Tr1F**, **Tr2F**, and **Tr3F** were estimated to be 3.14, 3.12, and 3.08 eV (Table S1), according to  $E_g = E_{ox} - E_{red}$ . The tendency matches well with their optical band-gaps ( $E_g^{opt}$ : 2.97, 2.86, and 2.85 eV for **Tr1F**, **Tr2F**, and **Tr3F**, respectively), which were obtained on the basis of the edges of the longest absorption wavelength of films. The results indicate that incorporating DPA end-groups can greatly raise HOMO energy levels, further adjusting the electrical characteristics to enhance the charge injection and transport properties.

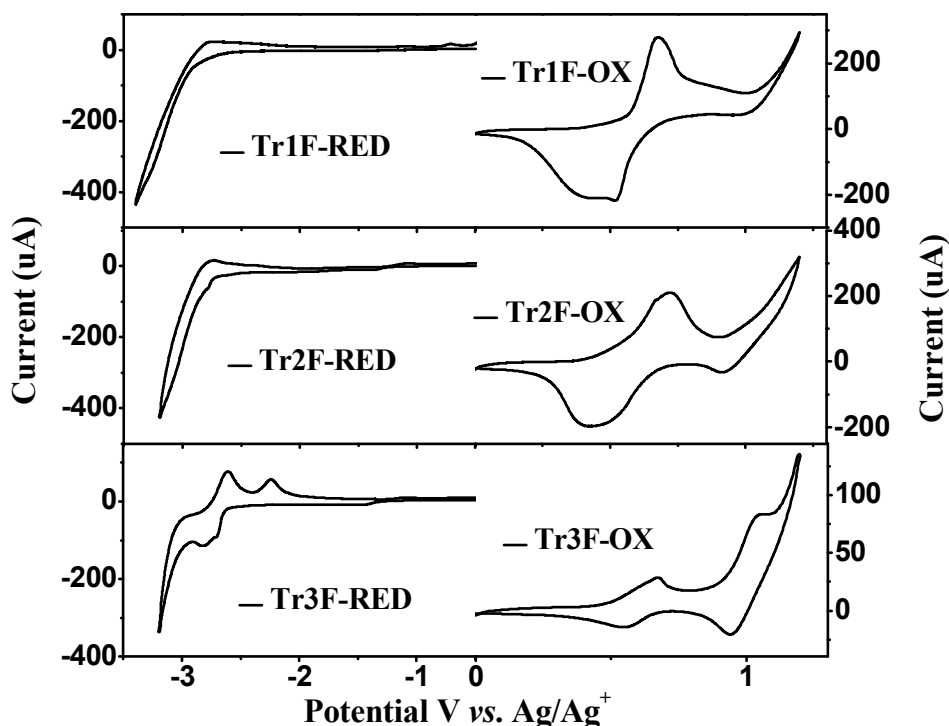


**Figure 4.** CV curves of **Tr1F**, **Tr2F**, and **Tr3F** in acetonitrile for oxidation and reduction.

### 3.4 Electroluminescence (EL) properties

With the aim to further study the EL characteristics of the six-armed conjugated starbursts, EL devices were manufactured with the construction of indium tin oxide (ITO)/PEDOT:PSS/Emissive layer (EML)/TPBI/LiF/Al. EML was spin-coated from chlorobenzene solutions (A: **Tr1F**; B: **Tr2F**; C: **Tr3F**). PEDOT:PSS and LiF was used as the hole-injection and electron-injection layer, respectively. As shown in Figure S30a-c, deep-blue emission was observed for **Tr1F**, **Tr2F**, and **Tr3F** at 437, 450, and 453 nm, respectively. As presented, the EL spectra maintained almost the same with their PL spectra in both solutions and solid states, implying that exciplex or excimer was greatly suppressed. Remarkably, the EL spectra maintained almost the same and the CIE coordinates were almost not varied with the increment of the driving voltages from 5 to 9 V. According to the results, EL emission is independent on the voltages, which probably results from the steric effect of the starbursts effectively depressing the molecular packing in films.

## WILEY-VCH

The current density–voltage–brightness ( $J$ – $V$ – $L$ ) characteristics, luminance efficiency–voltage ( $LE$ – $V$ ), and external quantum efficiency ( $EQE$ ) vs. current density curves of the devices are depicted in Figure S30d-f. OLEDs based on **Tr1F**, **Tr2F**, and **Tr3F** exhibited reduced turn-on voltages (3.2~3.5 V), which were much lower than those of their analogues without DPA end-groups (4.1~4.3 V for **Tr1-Tr3**).<sup>[38]</sup> This is mainly attributed to the incorporation of DPA end-groups that aid to raise the HOMO levels (from -5.66 eV ~ -5.74 eV for **Tr1-Tr3** to -5.17 ~ -5.22 eV for **Tr1F-Tr3F**), which are consistent with the anode work function (PEDOT:PSS/ITO, ~-5.2 eV) and thus enhance the hole-injection ability and charge balance. Superior device performance were obtained. Device A demonstrated good performance with a maximum luminance ( $L_{\max}$ ) of 1974 cd m<sup>-2</sup> (9.0 V), a maximum luminance efficiency ( $LE_{\max}$ ) of 2.28 cd A<sup>-1</sup>, and a maximum external quantum efficiency ( $EQE_{\max}$ ) of 2.00% (9.9 V, 393.4 mA cm<sup>-2</sup>, 1926.1 cd m<sup>-2</sup>). Improved performance was obtained from device B [ $L_{\max}$ : 2675 cd m<sup>-2</sup> (11.5 V),  $LE_{\max}$ : 2.61 cd A<sup>-1</sup>, and  $EQE_{\max}$ : 2.24% (11.3 V, 350.1 mA cm<sup>-2</sup>, 2665.2 cd m<sup>-2</sup>)] and device C [ $L_{\max}$ : 3478 cd m<sup>-2</sup> (9.4 V),  $LE_{\max}$ : 2.12 cd A<sup>-1</sup>, and  $EQE_{\max}$ : 1.85% (12.5 V, 760.1 mA cm<sup>-2</sup>, 2534.1 cd m<sup>-2</sup>)]. Apparently, the devices based on **Tr1F-Tr3F** achieved much better EL performance than that of **Tr1-Tr3** without DPA end-groups.<sup>[38]</sup> Besides, the devices based on **Tr1F-Tr3F** gave better performance than that of polyfluorene homopolymers end-capped with DPA units (ca. 1.1 cd/A at 1600 cd/m<sup>2</sup>).<sup>[47]</sup> Our results indicated that construction of DPA end-capped starbursts is beneficial to enhancing the electrical and luminous characteristics.

**Table 2.** EL characteristics of OLEDs from **Tr1F-Tr3F**.

Device	Compd	$V_{on}$ (V)	Luminance <sup>a)</sup> (cd m <sup>-2</sup> )	LE <sup>a)</sup> (cd A <sup>-1</sup> )	EQE <sup>a)</sup> (%)	CIE (x, y) at 6 V
A	<b>Tr1F</b>	3.4	1974	2.28	2.00	(0.16, 0.08)
B	<b>Tr2F</b>	3.2	2675	2.61	2.24	(0.16, 0.11)
C	<b>Tr3F</b>	3.5	3478	2.12	1.85	(0.17, 0.15)

<sup>a)</sup> Maximum values recorded from the devices.

The superior EL properties of these devices could result from reasons as follows: (1) the introduction of DPA are beneficial to raise HOMO energy levels; (2) the raised HOMO levels are in good agreement with the anode work function and thus promote the charge injection and transport; (3) the steric effect of starbursts can restrain the intermolecular interactions that aid to improve PL and EL ability; (4) the superior EL performance for device B based on **Tr2F** may originate from its proper molecular sizes and suitable HOMO and LUMO levels.

### 3.5 ASE and lasing characteristics

ASE spectra for **Tr1F-Tr3F** in films are depicted in Figure S31 in comparison with their absorption and PL spectra. With high excitation, the ASE peaks from **Tr1F**, **Tr2F**, and **Tr3F** are located at around 434, 443, and 450 nm, respectively. As far as we are concerned, the peaks correspond to the 0–1 vibrations, manifesting a quasi-four-level system for the film samples of **Tr2F** and **Tr3F**, which is beneficial to decreasing the ASE thresholds. The output intensity of edge emission is plotted as a function of the pump energy density (Figure 5a). The lowest  $E_{\text{th}}^{\text{ASE}}$  were recorded accordingly as 63.9 nJ pulse<sup>-1</sup> (3.5 μJ cm<sup>-2</sup> @ 498 nm) for **Tr1F**, 45.7 nJ pulse<sup>-1</sup> (2.5 μJ cm<sup>-2</sup> @ 489 nm) for **Tr2F**, and 27.4 nJ pulse<sup>-1</sup> (1.5 μJ cm<sup>-2</sup> @ 479 nm) for **Tr3F**, respectively. The results indicate that increasing the arm length aids to decrease the ASE thresholds.<sup>[37]</sup> Remarkably, **Tr3F** shows high fluorescence quantum yields, excellent morphology stability, and low ASE thresholds, which are comparable to the state-of-art blue organic lasers reported so far.<sup>[51,52]</sup> Based on the results, we speculate that the construction of starburst structures can effectively decrease the energy loss caused by molecular vibration and promote higher radiation transition efficiency, thus give superior ASE performance.

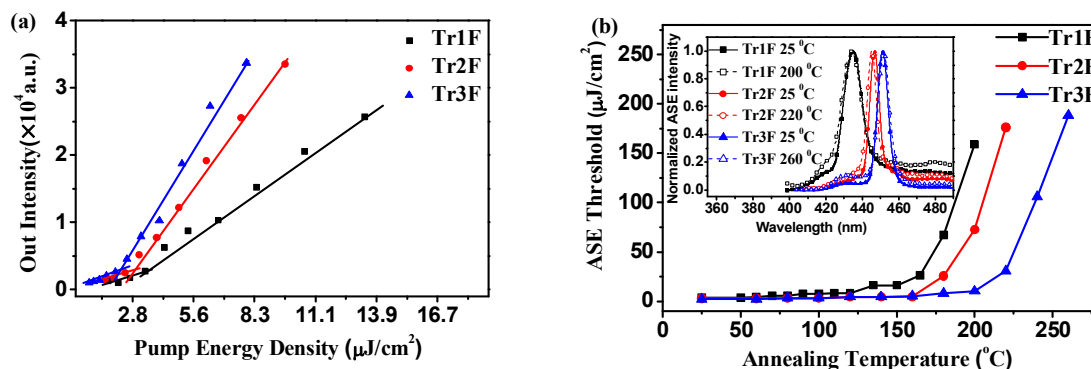


**Figure 5.** (a) The curves of ASE thresholds (r. t.) vs. pump energy density. (b) The curves of ASE thresholds vs. annealing temperature. The inset shows normalized ASE spectra at r. t. (solid line) and various annealing temperature (dashed line) under open ambient conditions.

The roadmap towards electrically pumped OSLs requires good thermal and optical stability of gain media. TGA and DSC measurements confirmed good thermal stability of these starbursts. For the purpose of further evaluating the photostability, the impact of annealing temperature on the ASE thresholds were studied (Figure 5b). During the test, the films were heated at different temperatures for 10 min under open ambient conditions. For each measurement, the excitation stripe was put to a different place on the specific sample for the purpose of eliminating the degradation of photodegradable molecules during the test. Most noticeably of all,  $E_{\text{th}}^{\text{ASE}}$  of **Tr1F** was enhanced twice compared with original samples by increasing room temperature to  $120^{\circ}\text{C}$ , while the annealing temperatures for **Tr2F** and **Tr3F** is up to  $160^{\circ}\text{C}$ . At the annealing temperature of  $200^{\circ}\text{C}$ , 50.3-fold and 10.1-fold of  $E_{\text{th}}^{\text{ASE}}$  were recorded for **Tr1F** and **Tr2F**, respectively, whereas only 5-fold was observed for **Tr3F**. It is worthwhile to mention that ASE of **Tr3F** can be detected even by heating at  $260^{\circ}\text{C}$ . The ASE spectra showed quite small shifts (around 4 nm) with the annealing temperature of  $220^{\circ}\text{C}$  and  $260^{\circ}\text{C}$  for **Tr2F** and **Tr3F**. Meanwhile, a small shift was also observed for **Tr1F** below  $200^{\circ}\text{C}$ , as depicted in the inset of Figure 6b. It is expected that the outstanding ASE thermal stability is beneficial for enhancing the optical gain stability to realize electrically pumped lasing.

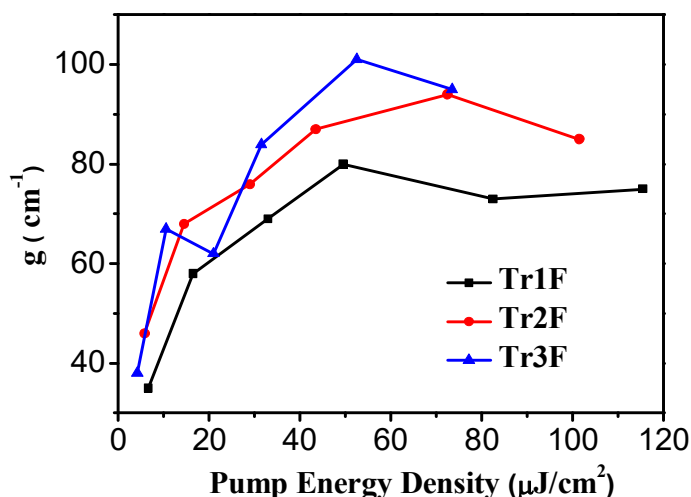


**Figure 6.** The plot of net gain coefficients ( $g$ ) as a function of different pumping intensity for **Tr1F–Tr3F**.

The variable stripe length (VSL) method is applied to study the optical gain properties. ASE emission intensity as a function of the stripe length with various pump intensities is plotted as shown in Figure S32. At the stripe lengths  $<2$  mm, by increasing the pump energy intensity, the output intensity exponentially increased, but then approached gain saturation at longer stripe lengths. To verify if the saturation resulted from the degradation, the characterization were carried out at the identical location repeatedly, and the results still remained. Before the gain grows saturated, by fitting the yielded results can obtain solid lines (Figure 6). The net gain was progressively enhanced by increasing the pump energy intensity; the light travelling in devices became magnified. With the emergence of gain saturation, no additional magnified light was obtained with the increase of the stripe length while the gain coefficient decreased. According to the data, the maxima net gain ( $g$ ) coefficients are calculated as  $80.1 \pm 2$ ,  $94.1 \pm 2$ , and  $101.3 \pm 2$   $\text{cm}^{-1}$ , with pump energy of 49.5, 72.5, and 52.5  $\mu\text{J cm}^{-2}$ , for **Tr1F**, **Tr2F**, and **Tr3F**, respectively.

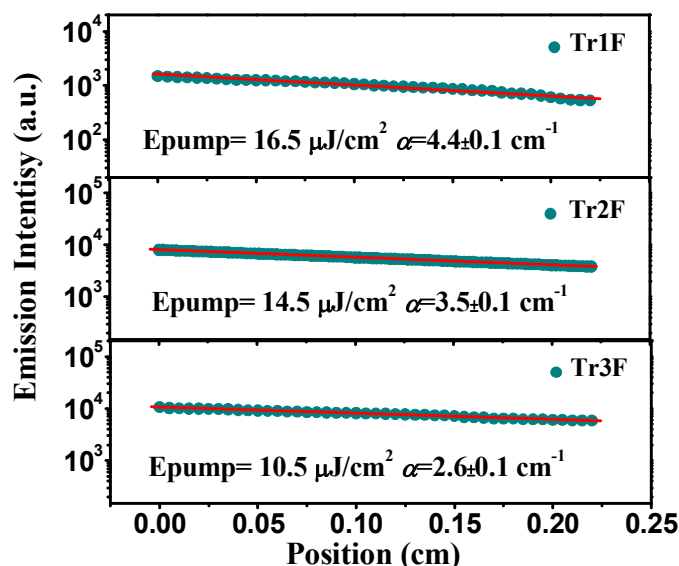
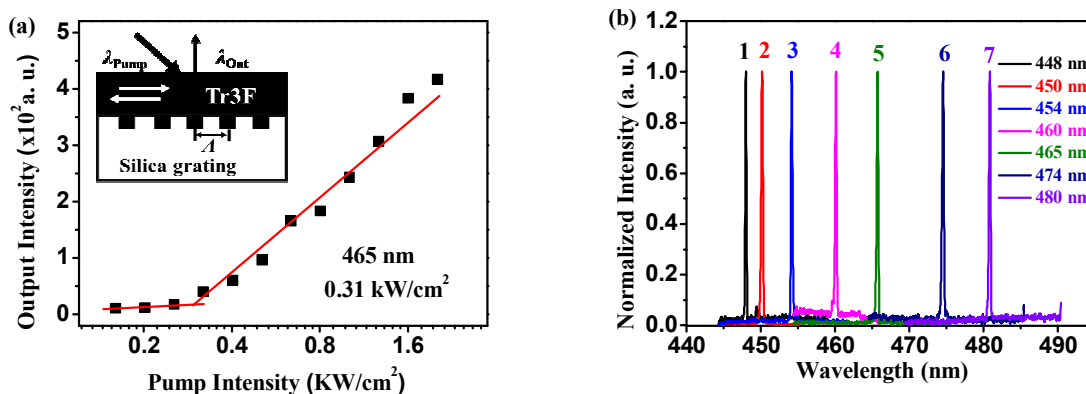


**Figure 7.** ASE loss coefficients of the waveguides for **Tr1F**, **Tr2F**, and **Tr3F**, respectively.

To gain deeper understanding about the optical gain characteristics of **Tr1F**, **Tr2F**, and **Tr3F**, the loss coefficients were calculated. Figure 7 shows the plot of loss coefficient versus stripe position. Low loss coefficients as  $4.4 \pm 0.1$ ,  $3.5 \pm 0.1$ , and  $2.6 \pm 0.1 \text{ cm}^{-1}$  were recorded for **Tr1F**, **Tr2F**, and **Tr3F**, respectively. Waveguide losses are attributed to absorption behaviors and scattering processes at the interfaces induced by surface roughness and large aggregates in the samples.<sup>[50]</sup> On the basis of the small loss coefficients, it is inferred that the resulting six-armed starbursts possess good waveguide properties and film-forming abilities. The low loss values and high gain render these materials rather promising as optical gain media for OSLs.



## WILEY-VCH

**Figure 8.** (a) Output intensity of **Tr3F** laser vs. pump energy. The detailed structure of the corresponding device is presented in the inset. (b) DFB lasing spectra of **Tr3F** possessing various film thickness and grating periods: (1) 160 nm with  $\Lambda = 280$  nm for  $\lambda = 448$  nm. (2) 180 nm with  $\Lambda = 280$  nm for  $\lambda = 450$  nm. (3) 200 nm with  $\Lambda = 280$  nm for  $\lambda = 454$  nm. (4) 160 nm with  $\Lambda = 290$  nm for  $\lambda = 460$  nm. (5) 180 nm with  $\Lambda = 290$  nm for  $\lambda = 465$  nm. (6) 160 nm with  $\Lambda = 300$  nm for  $\lambda = 474$  nm. (7) 180 nm with  $\Lambda = 300$  nm for  $\lambda = 480$  nm.

**Tr3F** was chosen as a typical material to study the lasing behaviors because of its smooth film morphologies and excellent ASE properties. One-dimensional distributed-feedback (DFB) gratings were prepared *via* nanoimprint lithography (NIL) methods. Second order gratings with 50% fill factor and 50 nm depth consisted of lines with periods of 280, 290, and 300 nm, respectively. As shown in Figure 8a, there emerged a sudden variation in the slope of the output intensity for **Tr3F** laser with the increment of excitation, which was recorded as the threshold. The minimum lasing threshold for **Tr3F** was  $0.31 \text{ kW cm}^{-2}$  ( $3.7 \text{ nJ pulse}^{-1}$ ) at 465 nm with a grating period of 290 nm. Moreover, FWHM of narrow lasing peaks were about 0.2 nm in DFB resonators. Generally, the lasing peaks strongly depend on the gratings and thickness of films. As depicted in Figure 8b, by simply modulating various gain layer thickness (160~200 nm) and grating periods (280, 290, 300 nm), the lasing spectra of **Tr3F** were adjustable ranging from 448 nm to 480 nm across a spectral window of 32 nm.

#### 4. Conclusions

To summarize, a novel set of monodisperse six-armed starbursts based on multibranched oligofluorenes with a truxene core and six DPA end-groups (**Tr1F**, **Tr2F**, and **Tr3F**) were designed and synthesized. As revealed by TGA, DSC, WAXD, optoelectronic, ASE and lasing characterizations, detailed studies were performed to provide a deep insight into the relationships between the electron-donating DPA end-groups and their corresponding optoelectronic properties. The resulting monodisperse six-armed starbursts manifested excellent thermal stabilities, facile

## WILEY-VCH

solution processability and pronounced PL efficiencies. The incorporation of peripheral DPA groups helps to increase the HOMO levels (0.49~0.52 eV higher than those of their analogues without DPA end-groups) and thereby enhance their hole-injection and transport. Noticeably, their raised HOMO energy levels consist with the anode work function, which thus facilitates the subsequent charge injection and transport. Consequently, relatively low turn-on voltages (3.2~3.5 V) and high luminescence (1974~3478 cd m<sup>-2</sup>) were achieved for the devices. By means of increasing the conjugation length of the six-armed starbursts, the ASE threshold decreases accordingly. Ultra-low ASE threshold about 27.4~63.9 nJ pulse<sup>-1</sup>, high net gain coefficients around 80.1~101.3 cm<sup>-1</sup>, outstanding ASE stability upon temperature, and low loss coefficients approximately 2.6~4.4 cm<sup>-1</sup> were recorded. Especially for **Tr3F** with the longest conjugation length, the films exhibited low  $E_{th}^{ASE}$  of 27.4 nJ pulse<sup>-1</sup> (2.1 μJ cm<sup>-2</sup> @ 479 nm), high net gain (101.3 cm<sup>-1</sup>), low loss (2.6 ± 0.1) cm<sup>-1</sup>, and excellent optical stability. Moreover, DFB lasers based on **Tr3F** exhibited lasing threshold of 0.31 kW cm<sup>-2</sup> (3.7 nJ pulse<sup>-1</sup>) at 465 nm in the case of a grating period of 290 nm. The results indicated that construction of DPA end-capped starburst oligofluorenes can effectively boost the electrical behaviors by raising the HOMO levels, and meanwhile, obviously improve their optical gain characteristics, endowing this kind of materials rather promising for attempting electrically pumped OSLs.

### Supporting Information

Supporting Information is available from the Wiley Online Library or from the author.

### Acknowledgements

We thank the National Natural Science Foundation of China (21835003, 21674050, 91833304, 21422402, 20904024), the National Key Basic Research Program of China (973 Program, 2014CB648300, 2017YFB0404501), the Natural Science Foundation of Jiangsu Province (BK20140060, BM2012010), Program for Jiangsu Specially-Appointed Professor (RK030STP15001), the Six Talent Peaks Project of Jiangsu Province (TD-XCL-009), the 333

## WILEY-VCH

Project of Jiangsu Province (BRA2017402), the NUPT "1311 Project" and Scientific Foundation (NY218164, NY217169, NY215062, NY217087), the Leading Talent of Technological Innovation of National Ten-Thousands Talents Program of China, the Excellent Scientific and Technological Innovative Teams of Jiangsu Higher Education Institutions (TJ217038), the Synergetic Innovation Center for Organic Electronics and Information Displays, and the Priority Academic Program Development of Jiangsu Higher Education Institutions (PAPD) for financial support.

Received: ((will be filled in by the editorial staff))

Revised: ((will be filled in by the editorial staff))

Published online: ((will be filled in by the editorial staff))

- [1] C. W. Tang, S. A. VanSlyke, *Appl. Phys. Lett.* **1987**, *51*, 913.
- [2] H. Uoyama, K. Goushi, K. Shizu, H. Nomura, C. Adachi, *Nature* **2012**, *492*, 234.
- [3] J. Yang, J. Huang, Q. Lia, Z. Li, *J. Mater. Chem. C* **2016**, *4*, 2663.
- [4] Q. Li, Z. Li, *Adv. Sci.* **2017**, *4*, 1600484.
- [5] A. J. C. Kuehne, M. C. Gather, *Chem. Rev.* **2016**, *116*, 12823.
- [6] J. R. Lawrence, G. A. Turnbull, I. D. W. Samuel, G. J. Richards, P. L. Burn, *Opt. Lett.* **2004**, *29*, 869.
- [7] N. Tessler, *Adv. Mater.* **1999**, *11*, 363.
- [8] L. H. Xie, C. R. Yin, W.-Y. Lai, Q. L. Fan, W. Huang, *Prog. Polym. Sci.* **2012**, *37*, 1192.
- [9] I. D. W. Samuel, E. B. Namdas, G. A. Turnbull, *Nat. Photonics* **2009**, *3*, 546.
- [10] Y. Yang, G. A., Turnbull, I. D. W. Samuel, *Appl. Phys. Lett.* **2008**, *92*, 163306.
- [11] Y. Yang, I. D. W. Samuel, G. A. Turnbull, *Adv. Mater.* **2009**, *21*, 3205.
- [12] D.-H. Kim, A. D'Aléo, X.-K. Chen, A. D. S. Sandanayaka, D. Yao, L. Zhao, T. Komino, E. Zaborova, G. Canard, Y. Tsuchiya, E. Choi, J. W. Wu, F. Fages, J.-L. Brédas, J.-C. Ribierre, C. Adachi, *Nat. Photonics* **2018**, *12*, 98.
- [13] C.-F. Liu, M. Sang, W.-Y. Lai, T.-T. Lu, X. Liu, W. Huang, *Macromolecules* **2018**, *51*, 1325.
- [14] T.-T. Lu, S.-J. Chang, Y.-Y. Liu, J.-Q. Pan, W.-Y. Lai, W. Huang, *Acta Polym. Sin.* **2018**, *2*, 304.

- [15] M. Morales-Vidal, P. G. Boj, J. M. Villalvilla, J. A. Quintana, Q. Yan, N. T. Lin, X. Z. Zhu, N. Ruangsupapichat, J. Casado, H. Tsuji, E. Nakamura, M. A. Diaz-Garcia, *Nat. Commun.* **2015**, *6*, 8458.
- [16] F. Montilla, R. Mallavia, *Adv. Funct. Mater.* **2007**, *17*, 71.
- [17] K. L. Chan, M. Sims, S. I. Pascu, M. Ariu, A. B. Holmes, D. D. C. Bradley, *Adv. Funct. Mater.* **2009**, *19*, 2147.
- [18] C. Poriel, N. Cocherel, J. Rault-Berthelot, L. Vignau, O. Jeannin, *Chem. Eur. J.* **2011**, *17*, 12631.
- [19] R. Xia, P. N. Stavrinou, D. D. C. Bradley, Y. Kim, *J. Appl. Phys.* **2012**, *111*, 123107.
- [20] T.-C. Lin, M.-L. Li, C.-Y. Liu, M.-Y. Tsai, Y.-H. Lee, Y. Febriani, J.-H. Lin, Y.-K. Shen, *Eur. J. Org. Chem.* **2014**, *2014*, 1615.
- [21] Y. Zhang, L. Chen, K. Zhang, H. Wang, Y. Xiao, *Chem. Eur. J.* **2014**, *20*, 10170.
- [22] H. Kim, N. Schulte, G. Zhou, K. Müllen, F. Laquai, *Adv. Mater.* **2011**, *23*, 894.
- [23] B. K. Yap, R. D. Xia, M. Campoy-Quiles, P. N. Stavrinou, D. D. C. Bradley, *Nat. Mater.* **2008**, *7*, 376.
- [24] S.-J. Chang, X. Liu, T.-T. Lu, Y.-Y. Liu, J.-Q. Pan, Y. Jiang, S.-Q. Chu, W.-Y. Lai, W. Huang, *J. Mater. Chem. C* **2017**, *5*, 6629.
- [25] W.-Y. Lai, R. Zhu, Q. L. Fan, L. T. Hou, Y. Cao, W. Huang, *Macromolecules* **2006**, *39*, 3707.
- [26] W.-Y. Lai, Q. Y. He, R. Zhu, Q. Q. Chen, W. Huang, *Adv. Funct. Mater.* **2008**, *18*, 265.
- [27] X. C. Li, C. Y. Wang, Y. Wan, W.-Y. Lai, L. Zhao, M. F. Yin, W. Huang, *Chem. Commun.* **2016**, *52*, 2748.
- [28] X.-C. Li, C.-Y. Wang, W.-Y. Lai, W. Huang, *J. Mater. Chem. C* **2016**, *4*, 10574.
- [29] X. C. Li, Y. Zhang, C. Y. Wang, Y. Wan, W.-Y. Lai, H. Pang, W. Huang, *Chem. Sci.* **2017**, *8*, 2959.
- [30] W.-Y. Lai, Q.-Y. He, Z. Ma, W. Huang, *Chem. Lett.* **2009**, *38*, 286.

- [31] Y.-D. Jiu, C.-F. Liu, J.-Y. Wang, W.-Y. Lai, Y. Jiang, W.-D. Xu, X.-W. Zhang, W. Huang, *Polym. Chem.* **2015**, *6*, 8019.
- [32] J.-M. Koenen, S. Jung, A. Patra, A. Helfer, U. Scherf, *Adv. Mater.* **2012**, *24*, 681.
- [33] F. Liu, W.-Y. Lai, C. Tang, H.-B. Wu, Q.-Q. Chen, B. Peng, W. Wei, W. Huang, Y. Cao, *Macromol. Rapid Commun.* **2008**, *29*, 659.
- [34] R. Xia, W.-Y. Lai, P. A. Levermore, W. Huang, D. D. C. Bradley, *Adv. Funct. Mater.* **2009**, *19*, 2844.
- [35] W. Xu, J. Yi, W.-Y. Lai, L. Zhao, Q. Zhang, W. Hu, X.-W. Zhang, Y. Jiang, L. Liu, W. Huang, *Adv. Funct. Mater.* **2015**, *25*, 4617.
- [36] M. Sang, S. Cao, J. Yi, J. Huang, W.-Y. Lai, W. Huang, *RSC Adv.* **2016**, *6*, 6266.
- [37] M. Fang, J. Huang, Y. Zhang, X. Guo, X. Zhang, C.-F. Liu, W.-Y. Lai, W. Huang, *Mater. Chem. Front.* **2017**, *1*, 668.
- [38] W.-Y. Lai, R. Xia, Q.-Y. He, P. A. Levermore, W. Huang, D. D. C. Bradley, *Adv. Mater.* **2009**, *21*, 355.
- [39] C. R. Belton, A. L. Kanibolotsky, J. Kirkpatrick, Clara Orofino, S. E. T. Elmasly, P. N. Stavrinou, P. J. Skabara, D. D. C. Bradley, *Adv. Funct. Mater.* **2013**, *23*, 2792.
- [40] H. Zhang, T.-T. Lu, W.-Y. Lai, X.-W. Zhang, M.-K. Zhang, P. Lv, C.-F. Liu, W. Huang, *J. Phys. Chem. C* **2017**, *121*, 27569.
- [41] Q. D. Liu, J. P. Lu, J. F. Ding, M. Day, Y. Tao, P. Barrios, J. Stupak, K. Chan, J. J. Li, Y. Chi, *Adv. Funct. Mater.* **2007**, *17*, 1028.
- [42] P. L. Wu, X. J. Feng, H. L. Tam, M. S. Wong, K. W. Cheah, *J. Am. Chem. Soc.* **2009**, *131*, 886.
- [43] T. Qin, W. Wiedemair, S. Nau, R. Trattnig, S. Sax, S. Winkler, A. Vollmer, N. Koch, M. Baumgarten, E. J. List, K. Müllen, *J. Am. Chem. Soc.* **2011**, *133*, 1301.
- [44] M. P. Aldred, C. Li, G. F. Zhang, W. L. Gong, A. D. Q. Li, Y. F. Dai, D. G. Ma, M. Q. Zhu, *J. Mater. Chem.* **2012**, *22*, 7515.

- [45] G. Zhang, M. Baumgarten, M. Auer, R. Trattnig, E. J. List-Kratochvil, K. Müllen, *Macromol. Rapid Commun.* **2014**, *35*, 1931.
- [46] R. Muangpaisal, M.-C. Ho, T.-H. Huang, C.-H. Chen, J.-Y. Shen, J.-S. Ni, J. T. Lin, T.-H. Ke, L.-Y. Chen, C.-C. Wu, C. Tsai, *Org. Electron.* **2014**, *15*, 2148.
- [47] T. Miteva, A. Meisel, W. Knoll, H. G. Nothofer, U. Scherf, D. C. Müller, K. Meerholz, A. Yasuda, D. Neher, *Adv. Mater.* **2001**, *13*, 565.
- [48] L. Yu, J. Liu, S. Hu, R. He, W. Yang, H. Wu, J. Peng, R. Xia, D. D. C. Bradley, *Adv. Funct. Mater.* **2013**, *23*, 4366.
- [49] A. J. C. Kuehne, M. C. Gather, *Chem. Rev.* **2016**, *116*, 12823.
- [50] H. Ma, A. K. Y. Jen, L. R. Dalton, *Adv. Mater.* **2002**, *14*, 1339.
- [51] L. Bai, B. Liu, Y. Han, M. Yu, J. Wang, X. Zhang, C. Ou, J. Lin, W. Zhu, L. Xie, C. Yin, J. Zhao, J. Wang, D. D. C. Bradley, W. Huang, *ACS Appl. Mater. Interfaces* **2017**, *9*, 37856.
- [52] D.-H. Kim, A. S. D. Sandanayaka, L. Zhao, D. Pitrat, J. C. Mulatier, T. Matsushima, C. Andraud, J. C. Ribierre, C. Adachi, *Appl. Phys. Lett.* **2017**, *110*, 023303.

**Monodisperse six-armed starburst conjugated molecules with diphenylamine (DPA) end-cappers are synthesized, and their optical gain and lasing characteristics have been investigated.** The incorporation of DPA end-groups effectively raises the HOMO levels thus effectively enhancing the hole injection and transport ability. The resulting starbursts manifested stabilized optical gain and lasing performance with low thresholds ( $27.4\sim 63.9\text{ nJ pulse}^{-1}$ ), high net gain coefficients ( $80.1\sim 101.3\text{ cm}^{-1}$ ) and small waveguide loss ( $2.6\sim 4.4\text{ cm}^{-1}$ ).

### Organic Semiconductor lasers

*H. Zhang, X. Liu, T.-T. Lu, P. Lv, and W.-Y. Lai\**

### Monodisperse Six-Armed Starbursts based on Truxene-Cored Multibranching Oligofluorenes: Design, Synthesis, and Stabilized Lasing Characteristics

